Oscillatory instabilities during formic acid oxidation on Pt(100), Pt(110) and Pt(111) under potentiostatic control. I. Experimental

Cite as: J. Chem. Phys. **107**, 979 (1997); https://doi.org/10.1063/1.474450
Submitted: 16 December 1996 . Accepted: 08 April 1997 . Published Online: 04 June 1998

P. Strasser, M. Lübke, F. Raspel, M. Eiswirth, and G. Ertl

Oscillatory instabilities during formic acid oxidation on Pt(100), Pt(110) and Pt(111) under potentiostatic control. I. Experimental

P. Strasser,[a] M. Lübke, F. Raspel, M. Eiswirth, and G. Ertl
Fritz-Haber-Institut der Max-Planck-Gesellschaft, Faradayweg 4-6, D-14195 Berlin, Germany

(Received 16 December 1996; accepted 8 April 1997)

The experimental characterization of the current/outer potential (I/U) behavior during the electrochemical CO oxidation on Pt(100), Pt(110) and Pt(111) is used as the first step towards a thorough investigation of the processes occurring during the electrochemical formic acid oxidation. The CO study is followed by new cyclovoltammetric results during the electrochemical formic acid oxidation on the corresponding Pt single crystals. At high concentrations of formic acid, the cyclovoltammograms revealed a splitting of the large current peak observed on the cathodic sweep into two peaks whose dependence on scan rate and reverse potential was investigated. It turned out that the presence of a sufficiently large ohmic resistance R was crucial for oscillatory instabilities. Given an appropriate resistance, all three Pt surfaces were found to exhibit current oscillations at both low and high formic acid concentrations. On Pt(100) stable mixed-mode oscillations were observed. In addition, the sensitivity of the oscillations to stirring was investigated. Whereas the period-1 oscillations were found to be independent of stirring, the mixed-mode oscillations transformed into simple oscillations with stirring. The mechanism giving rise to instability and oscillations is described. © *1997 American Institute of Physics.* [S0021-9606(97)01227-0]

I. INTRODUCTION

The first observation of temporally periodic instabilities during the electrocatalytic oxidation of formic acid (HCOOH) dates back almost 70 years.[1] Ever since these early experiments, more and more experimental methods have been applied to elucidate the oscillatory processes occurring in the system and numerous speculations on the origin of the instabilities have been put forward.

Instabilities in electrochemical systems can be subdivided into two classes:[2] One class includes purely chemical instabilities, i.e., instabilities which arise from chemical kinetics. The electrode potential is not an essential variable for these kinds of instabilities. The second class of instabilities, however, requires the interplay of chemical and electrical variables; they disappear as soon as the electrode potential is kept constant. We will discuss instabilities of the latter type only, and give evidence why the first class can be neglected in the formic acid system.

As for the origin of electrochemical instabilities, Degn[3] and De Levie[4] were among the first to emphasize the possibly important role of a negative slope in the current/potential curve (I/U) as well as a sufficiently large ohmic resistance R in series with the electrochemical cell. The effect of an ohmic resistance is as follows: Assuming a constant outer potential U given between reference and working electrode of an electrochemical cell and a current I flowing through the system, the ohmic resistance R causes U to be split into the potential drop across the double layer, henceforth referred to as ϕ_{dl}, and into an additional potential drop commonly referred to as the IR drop. Only the potential ϕ_{dl} determines the actual electrochemical processes occurring at the electrode. Recently, Koper revived and extended the early ideas on electrochemical instabilities;[5–8] he pointed out that an electrochemical system becomes unstable towards small potential perturbations if there exists some potential interval characterized by a negative differential resistance $Z_F = dI/d\phi$ and a sufficiently large ohmic resistance R which fulfills the condition $R > |Z_F|$. According to Koper a negative Z_F can be caused by the ad/desorption of a chemical activator/inhibitor, a poisonous intermediate or by electrostatic effects between electroactive species and the electrode. The simplest type of instability manifests itself by the coexistence of two stable stationary states (e.g., current values I in the case of an electrochemical system) for the same value of a system parameter (e.g., outer potential U). Koper further showed that in the presence of slow mass transport processes, not only bistability but also oscillatory instabilities can be obtained in electrochemical systems.

Conditions of electrochemical measurements for vanishing ohmic resistance R are commonly referred to as *truly potentiostatic conditions*, since $\phi_{dl} = U = \text{const}$. In contrast, if R is finite, ϕ_{dl} may vary considerably from the fixed outer potential U; such conditions are called *potentiostatic with fixed outer potential* and are mostly employed in Section II.

Early work on oscillatory instabilities during formic acid (FA) oxidation was performed on polycrystalline electrodes of Rh, Pt and Pd under galvanostatic control.[1,9,10] Finally, an important step towards an understanding of the relevant chemical processes was achieved when single crystals, predominantly Pt, were introduced as working electrodes.[11–19]

There are only a few studies dealing with oscillations of the measured current during FA oxidation on low-index Pt single crystals[15–19] under potentiostatic control. These studies provide similar physicochemical interpretations of the current oscillations assuming formic acid to be oxidized via a direct and an indirect reaction path (dual-path mechanism[20]).

[a]Electronic mail:peter@pippi.rz-berlin.mpg.de

The periodic adsorption and reactive removal of CO by adsorbed oxygen species (possibly combined with periodic changes in the surface structure[17] or the local pH[15,16,19]) is identified with the experimental current oscillations. In Refs. 17 and 19, the authors propose an autocatalytic removal of CO in order to account for the observed instabilities, whereas Refs. 15 and 16 found the FA oxidation mechanism to contain unstable network features. So, all potentiostatic FA studies emphasized purely chemical sources of instability, whereas the role of an ohmic resistance R was not explicitly considered.

The potentiostatic studies are in agreement as to the significant difference between the single crystal planes, but differ considerably in the results concerning the role of mass transport and the local pH. Pt(100) was found to reproducibly show current oscillations, whereas on Pt(110) and Pt(111) oscillatory behavior was difficult to obtain.

In the present study, we present new results on current oscillations during FA oxidation occurring on the three low-index Pt planes. First, however, we want to look into the current/potential behavior of the electrochemical CO oxidation (Section III) which can be considered as a subsystem of the FA system. In Section IV, we first consider the current/potential characteristics during formic acid oxidation on Pt(100), Pt(110) and Pt(111) at low ohmic resistance before addressing the complex oscillatory instabilities seen in the cyclovoltammograms (CVs) at higher ohmic resistances. Furthermore, we focus on current oscillations and, finally, report the observed effects when stirring is applied to current oscillations.

II. EXPERIMENT

All experiments were performed in a conventional three-compartment electrochemical cell. One compartment contained a Pt wire as counterelectrode; a Hg/Hg_2SO_4 electrode served as reference electrode in the second compartment. In the following, however, all given potentials refer to the standard calomel electrode (SCE). The distance between reference and working electrode was kept small (<3 mm) by means of a Luggin capillary.[16] In the main compartment low-index Pt single crystals Pt(100), Pt(110) and Pt(111) (≈ 0.6 cm^2 each) were used as working electrodes. The working electrode was first dipped into the electrolyte and then pulled out as far as possible thereby avoiding crystal edge effects.[21]

The pretreatment of the single crystals was as follows: First, the single crystals were annealed at 1500 K in a Bunsen flame for about 1 min. The crystals were then cooled in an N_2 atmosphere for at least 5 min and rapidly transferred into the electrochemical cell.[22] Flame annealing became necessary whenever the applied sweep potentials reached values where surface roughening sets in.

All electrolyte solutions (1 M Na_2SO_4 saturated with gaseous CO for the CO oxidation experiments and 0.05 M HCOOH in 10^{-3} M $HClO_4$ and 1 M HCOONa in 0.5 M H_2SO_4 for experiments involving formic acid) were prepared with tridistilled water. H_2SO_4 and $HClO_4$ (Merck) were purchased as suprapure chemicals and were used without further purification. HCOOH, HCOONa, Na_2SO_4,$NaClO_4$ and NaOH were employed with p.A. purity. Before each measurement of Section III, first a N_2 (5 N) gas stream was bubbled through the solution in order to remove dissolved oxygen. Thereafter, CO (4.7 N) gas was extensively bubbled through the electrochemical cell to achieve saturation. The gas stream was maintained during CO oxidation experiments ensuring a CO atmosphere. The degree of saturation was monitored by means of the measured current densities. In order to match the pH conditions of the formic acid experiments, the CO saturated solution was set to $pH \approx 2.7$ using sulphuric acid. Before and during the experiments on formic acid, a N_2 gas stream was bubbled through the cell electrolyte in order to keep the cell free of air.

Stirring was achieved by means of a magnetic stirrer sitting on the bottom of the cell. The measurements were performed at room temperature throughout.

III. ELECTROCHEMICAL CO OXIDATION

There is significant evidence that the electrochemical formic acid oxidation partially proceeds via a surface poison which is oxidized by oxygen-containing species forming at higher double-layer potentials. The poisonous intermediate was recently identified as CO.[23–25] Consequently, the electrochemical CO-oxidation system can be thought of as a simple submechanism of that of formic acid oxidation. In the following we report experiments on CO oxidation in solution of high ionic conductivity (1 M Na_2SO_4) in order to avoid any electrochemical instabilities.

Figure 1 shows the scanned I/U curves of the three low-index Pt single crystals Pt(100), Pt(110) and Pt(111) for two different upper limit potentials. All three surfaces are seen to exhibit two different states for small and high values of the outer potential U, respectively: At low potentials of U, the surface is poisoned by CO and the current density vanishes, whereas at higher values of U oxygen-containing species deactivate the surface. The blockage of the surface by oxygen species, however, is not complete in the potential range considered, since a current is observed in the high-potential state suggesting an ongoing diffusion-limited oxidation of CO despite oxygen inhibition. Between the two constant current plateaus a sharp CO-oxidation peak is visible on the anodic scan, whereas a smoother transition occurs sweeping cathodically towards the CO covered state. One immediately recognizes that the potential range over which the CO poisoning occurs on the cathodic scan is shifted towards smaller values of U compared to the potential range of CO removal during the anodic scan. This effect remains even for turning potentials right past the CO-oxidation peak indicating that it is not entirely due to irreversible oxide formations. At first sight, this behavior suggests the coexistence of two values of I for one given value of U. In order to doublecheck for such a coexistence, the CO-oxidation system was subject to galvanostatic conditions: As the current was increased in small increments from zero up to the diffusion limiting current of Fig. 1, no value of I could be found for which U decreased with increasing I (negative I/U characteristic). Such a char-

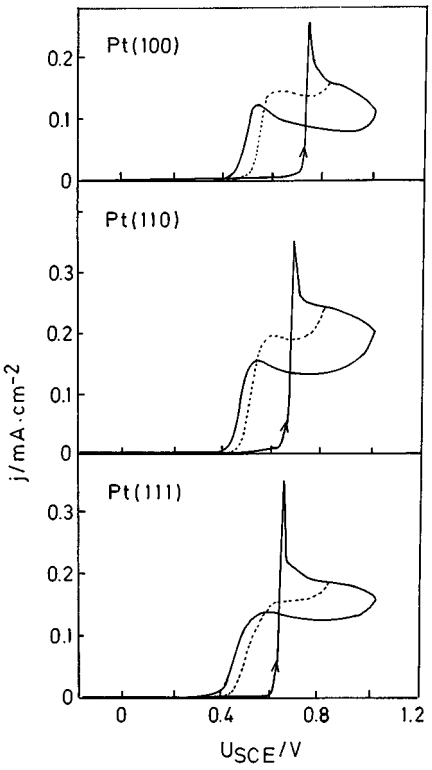

FIG. 1. Experimental cyclovoltammograms (CVs) of the CO oxidation at Pt(100), Pt(110) and Pt(111) single crystal surfaces. The dashed curve shows the cathodic backscan obtained with a lower turning potential. Electrolyte: 1 M Na_2SO_4, pH 2.7, saturated with CO, scan rate 10 mV/s, magnetic stirring.

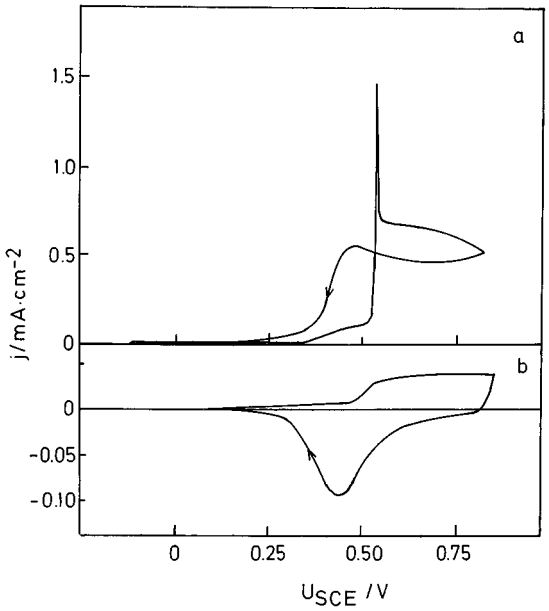

FIG. 2. (a) Experimental CVs of the CO oxidation and (b) the OH adsorption and desorption on a rotating disk electrode (Pt poly) with stirring of 3000 rpm, scan rate 20 mV/s. Electrolyte: 1 M Na_2SO_4, pH 2.7; saturated with CO (a), saturated with N_2 (b).

acteristic corresponding to the potentiostatically unaccessible, unstable steady-state branch is expected in the presence of a true potentiostatic bistability. Instead, there was an identical, reversible one-to-one correspondence between current values I and the outer potentials U in both scan directions.

The stationary measurements reveal that the I/U behavior of CO removal coincides under scanned and stationary conditions, whereas the CO poisoning is shifted to higher values of U in the stationary case.

Figure 1 further reveals that the CO oxidation peak does not coincide for the three single crystals. Instead, the current I rises at increasingly smaller values of U on the anodic sweep going from Pt(100) to Pt(110) and to Pt(111).

For the sake of comparison, Fig. 2 shows a typical I/U behavior of the CO system on a rotating polycrystalline Pt electrode. Here, the mass transport is much better defined compared to magnetic stirring. The values of current densities are higher; however, the overall behavior of the electrochemical system is seen to be qualitatively unchanged.

IV. ELECTROCHEMICAL HCOOH OXIDATION

We report cyclovoltammetric measurements on Pt(100), Pt(110) and Pt(111). The cyclovoltammograms are complemented by measurements of the temporal evolution of the current I for a constant potential U. Except for the upcoming section on stirring effects, all CVs and current oscillations were measured without stirring the electrolyte.

A. *I/U* characteristics at low ohmic resistances

Figure 3 shows the CVs of the three single crystal surfaces at a scan rate of 10 mV/s in a solution of high ion conductivity, i.e., almost vanishing ohmic resistance R.

One recognizes the typical current-potential characteristics of self-poisoning oxidation reactions of small organic compounds.[16,18,19,23] Starting at low values of the outer potential U, Pt(100) and Pt(110) show a very similar behavior: a high degree of poisoning of the surface in the potential region 0.2–0.5 V results in a low current density. The small peak observed in this region will be referred to as peak I.[20,26] At higher values of U (0.55–0.6 V), adsorption with oxygen

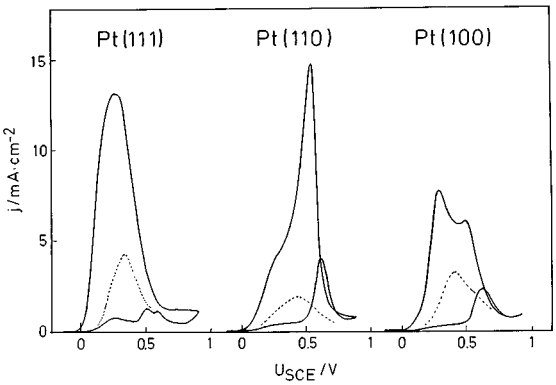

FIG. 3. I/U characteristics for the oxidation of FA on the three Pt single crystal surfaces. Electrolyte: 1 M HCOONa + 0.5 M H_2SO_4, pH 2.6 , without stirring. Solid curve: scanned with 10 mV/s, dashed curve: stationary behavior.

species (OH) starts leading to an activation of the surface by oxidation of the poisoning species. The current increases considerably. In the following, this current peak will be referred to as peak II.[26] Further increase of U up to 0.8–0.9 V leads back to a deactivated surface due to the coverage of oxygen species. Note that the current density does not decrease back to the values where it started when the surface was poisoned. Instead, the current stays at around 1 mA/cm^2 indicating an incomplete inhibition of formic acid oxidation by the OH coverage. At considerably higher values of U, a third anodic peak (peak III) occurs[20,27] which, however, will not be considered in this study since the potential sweep was reversed as soon as the surface had been deactivated past peak II.

On the reversed scan of Pt(100) and Pt(110), the surface gets reactivated very rapidly as soon as the OH species desorb (0.6–0.5 V). Now, the surface is almost free of poisoning species and the oxidation of formic acid proceeds in an unhindered manner which leads to a large current peak referred to as peak IV. Scanning to more negative potential, however, the CV reveals another current peak around 0.25 V for both Pt(100) and Pt(110) (referred to as peak V). Whereas on Pt(100) peak IV is smaller than peak V, the reverse holds for Pt(110), where peak V appears as a shoulder of peak IV.

In contrast to Pt(100) and Pt(110), Pt(111) shows a distinct peak I and a small split peak II. Furthermore, on the cathodic scan there is no separation between peaks IV and V. Instead, both peaks merge into one broad current peak.

Further investigation of the characteristics of peaks IV and V revealed a complex dependence of both peaks on the scan rate and the anodic limit potential: Figs. 4(a) and 4(b) show the dependence of peak IV and peak V on the upper limit potential. The negative portion of the I/U curve of the pure electrolyte without formic acid is shown in Fig. 4(c) to compare the potential regions of peak IV and V and the potential at which the deposited (ir) reversible surface oxides are reduced. The experiments suggest a strong increase of peak IV with the upper turning potential (going from dotted, dashed to solid) on both surfaces [on Pt(110) even more drastic than on Pt(100)]. The effect of the turning potential on peak V, however, differs significantly on Pt(100) and Pt(110): Whereas an increase in turning potential leads to a small decrease of the shoulderlike peak V on Pt(110), it results in a moderate increase of peak V on Pt(100). Figure 4(c) again confirms that peak IV occurs at values of U, where the rate of desorption/reduction of OH reaches its maximum.

On Pt(100) as well as on Pt(110), peak IV was found to increase at higher sweep rates; peak V, however, remained unchanged on Pt(110), but increased on Pt(100).

Looking at the CVs of Figs. 4 and 3 one might be tempted to conclude from the different current densities during the anodic and cathodic scan that there is a bistability somewhere in the considered potential interval. The stationary I/U curves, however, (dotted line in Fig. 3) reveal the kinetic nature of the differences in current densities. If one stops the potential sweep on peak IV, for instance, the current eventually decreases down to the dotted line. For each

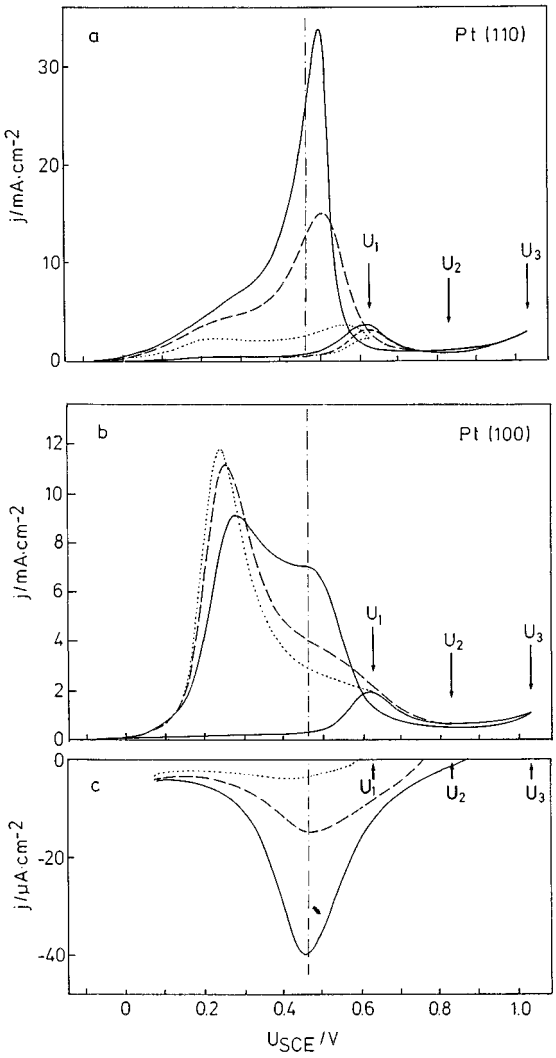

FIG. 4. I/U curves of the FA oxidation (a) and (b), and OH desorption (c) at Pt(110) and Pt(100). Electrolyte: 1 M HCOONa + 0.5 M H_2SO_4, pH 2.6 (a) and (b), 1 M Na_2SO_4, pH 2.6. The scan (20 mV/s) was reversed at different anodic potentials as indicated by the arrows.

value of U there exists exactly one value of I. Thus, in agreement with what has been pointed out in Sec. I there is no electrochemical instability present in the system for a small value of R.

B. Instabilities at high values of *R*

In Sec. I, a general argument has been given in order to explain the instability occurring at sufficiently high values of R. Figure 5 illustrates this idea schematically for the CV of Pt(100) given in Fig. 3(c) and provides a qualitative explanation of the observed shapes of the CV. In Fig. 5(a), the CV of Pt(100) is shown without an additional external series resistance R_{ex}. Increasing R_{ex} and correcting the CV by the value of the IR drop results in the distortion of the original CV as can be seen by the dotted line in Figs. 5(b) and 5(c). Note that the dotted $I-U$ curve is not entirely accessible, i.e., does not correspond to a real CV. Instead, the solid line in Figs. 5(b) and 5(c) schematically sketches out the CV that

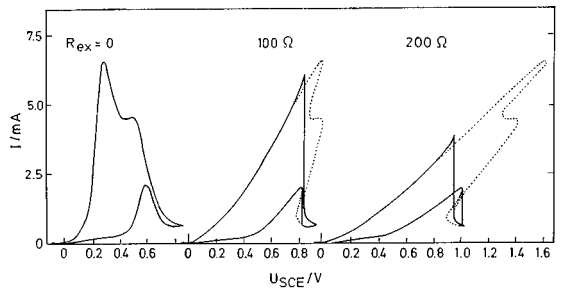

FIG. 5. Effect of an increasing external ohmic resistance R_{ex} on an experimental CV of the FA oxidation reaction measured in solution of high ionic conductivity and with $R_{ex}=0, U\approx\phi$. (a) shows the experimental CV on Pt(100) in 1 M HCOONa, 0.5 M H_2SO_4, scan rate 10 mV/s (see Fig. 3). (b) and (c) display the calculated I/U curves according to $U=\phi+IR$ for $R_{ex}=100\ \Omega$ and $R_{ex}=200\ \Omega$, respectively as dashed curves. The experimental CVs expected in the presence of an external ohmic resistance [cases (b) and (c)] are shown by the solid curves. It is seen that some parts of the dashed curve are not accessible experimentally. Furthermore, the generation of a hysteresis (bistability) is observed in the solid scanned curves at a sufficiently high value of R_{ex}.

one would measure during a cathodic and anodic potential scan if no oscillatory instabilities were present. Scanning anodically, one can see that peak II becomes strongly asymmetric; at the turning point the current falls off abruptly to low values. On the reversed scan in Fig. 5(c), the current remains low even beyond the potential at which the current fell off from peak II. At even lower potential the current increases again abruptly and follows the dotted curve down to low values of U. Thus, bistability is generated with a sufficiently large external resistance.

Figure 6 shows the measured $I-U$ curves for the three single crystal surfaces at a concentration of 0.05 M HCOOH in 10^{-3} M $HClO_4$. In accordance with the previous paragraph, all CVs are distorted towards slightly higher values of U as compared to the curves of Fig. 3. For Pt(100) high current spikes occur on the cathodic scan, whereas Pt(110) exhibits high frequency spikes on peak II. Pt(111), in contrast, does not show any spiking.

In order to determine whether the ohmic resistance of the electrolyte is crucial for the observed instabilities, the

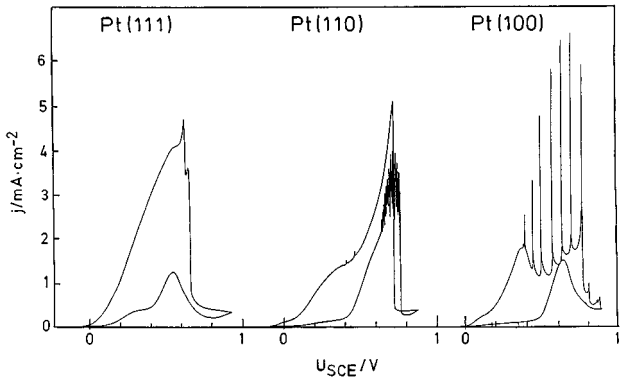

FIG. 6. CVs of FA oxidation on the three Pt single crystal surfaces at low concentrations of FA and of the bulk electrolyte: 0.05 M HCOOH, 10^{-3} M $HClO_4$, scan rate 10 mV/s.

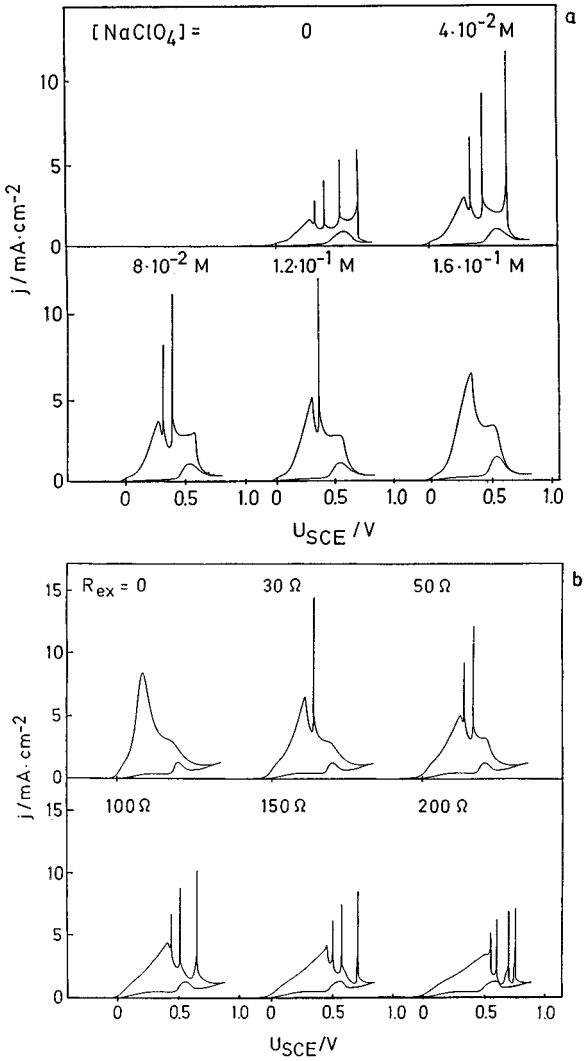

FIG. 7. (a) CVs of FA oxidation on Pt(100) for increasing ionic conductivity of the bulk electrolyte in the absence of any external resistance. Initial bulk solution: 0.05 M HCOOH, 10^{-3} M $HClO_4$. Increase in conductivity is achieved by addition of different amounts of $NaClO_4$. Scan rate 10 mV/s throughout. (b) CVs of FA oxidation on Pt(100) for increasing external ohmic resistances. Bulk solution: 1 M HCOONa, 1 M HCOOH, pH 3.0. Scan rate 10 mV/s throughout.

$I-U$ characteristics of Pt(100) [Fig. 6(c)] were monitored for decreasing values of R. The decrease of R was achieved by the successive addition of $NaClO_4$. In Fig. 7(a), one clearly sees how the current spikes disappear as the ohmic resistance is decreased. After the addition of 1.6×10^{-1} M $NaClO_4$ the CV of Pt(100) equals the one shown in Fig. 3(c). Conversely, in Fig. 7(b) it is shown that starting with a CV of Pt(100) similar to that given in Fig. 3(c) and increasing the ohmic resistance R by adding an external resistor R_{ex} one induces the current spikes which indicate instability. It can be concluded that the observed instabilities require a sufficiently large ohmic resistance R.

C. Current oscillations at fixed values of *U*

1. Low HCOOH concentration

Unless stated otherwise, the bulk electrolyte used in the following contained 0.05 M HCOOH and 10^{-3} M $HClO_4$.

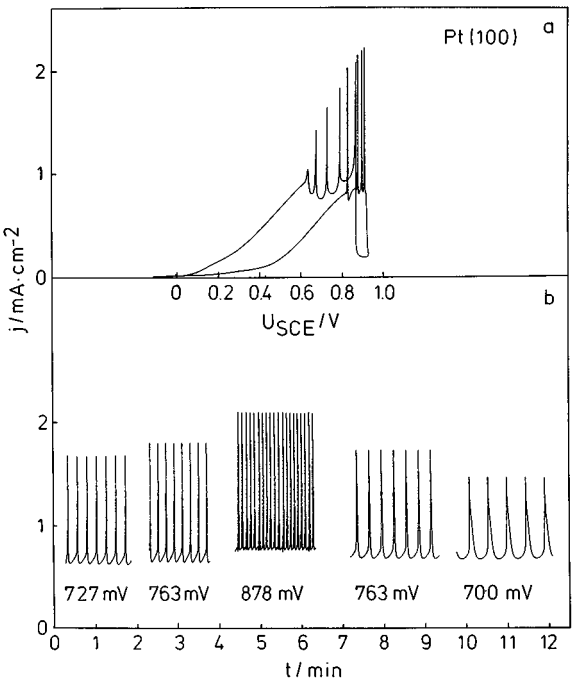

FIG. 8. (a) CV of FA oxidation on Pt(100) with external resistance $R_{ex}=600\ \Omega$ at low FA concentration. Bulk solution: 0.05 M HCOOH, 10^{-3} M $HClO_4$. Scan rate 5 mV/s. Sharp current spikes appear on both the anodic and the cathodic scan indicating oscillatory behavior of the current. (b) Current oscillations after holding the scan at different potentials U. From left to right, the first three times series were obtained when stopping on the anodic scan, the remaining two ones when stopping on the cathodic scan.

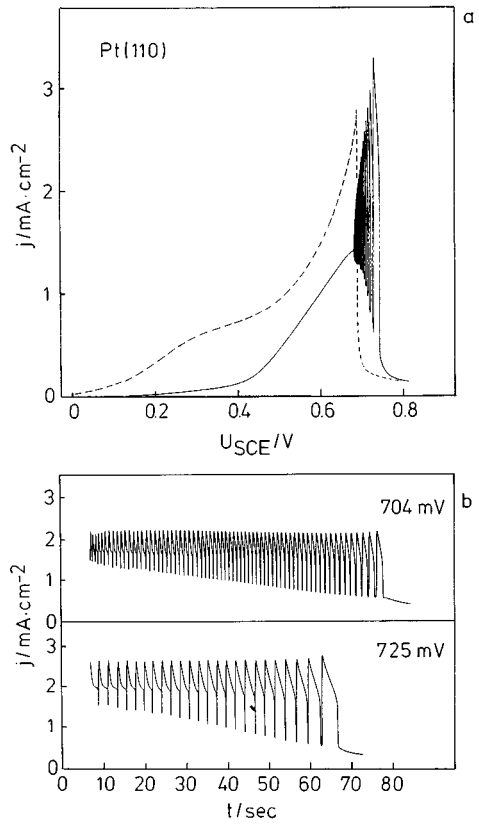

FIG. 9. (a) CV of FA oxidation on Pt(110) with external resistance $R_{ex}=80\ \Omega$ at low FA concentration. Bulk solution: 0.05 M HCOOH, 10^{-3} M $HClO_4$. Scan rate 5 mV/s. Sharp current spikes appear on the anodic scan only. (b) Current oscillations when the scan was stopped at 704 and 725 mV.

During most measurements an additional external resistor R_{ex} was used in series with the electrochemical cell.

Pt(100). Figure 8(a) depicts the measured CV with $R_{ex}=600\ \Omega$. On the cathodic scan there are the current spikes as in Fig. 6, but now there are also current spikes visible on peak II indicating a regime of current oscillations. A small region of bistability is discernible between the potential of reactivation on the cathodic scan and the potential of oxygen blocking past peak II. To check a possible correspondence of the oscillatory potential range of both scan directions, the anodic scan was stopped at different potentials on the ascending flank of peak II. In fact, stable relaxational current oscillations were finally obtained where a smooth curve has been obtained when scanning. Figure 8(b) directly contrasts the wave forms of the current oscillations obtained when holding the potential in the anodic and the cathodic scan. The qualitative agreement of the oscillatory wave forms is clearly seen. The oscillations are characterized by a gradual increase of the current density followed by a very rapid decrease due to the poisoning reaction. Furthermore, the oscillations at higher values of U are more relaxational and of larger amplitude than those at lower values of U indicating a Hopf bifurcation at low values of U.

Pt(110). In Fig. 9(a) a CV of the (110) surface is given with $R_{ex}=80\ \Omega$. The anodic scan is drawn as a solid line, whereas for the sake of clarity the reverse is shown as a dashed line. Similar to Fig. 6(b), there is a potential region on peak II where high-frequency current spikes occur. No current spikes are seen on the cathodic scan. Fixing the potential inside the current spike region, leads to transient current oscillations as given in Fig. 9(b) for $U=704$ and $U=725$ mV. The lifetime of the oscillations is about 1 min. Thereafter, the current remains low due to high OH coverage. Looking at the wave form of the oscillations, one recognizes a delayed current decrease, i.e., a slower poisoning process as compared to Pt(100), but a very rapid increase in current density.

Pt(111). In contrast to the CV given in Fig. 6(a), the CV shown in Fig. 10(a) was recorded with $R_{ex}=430\ \Omega$. Several broad current spikes can be seen on the ascending flank of peak II. No spikes could be observed on the cathodic scan. Here, the hysteresis of the transition between a predominantly CO-covered surface and a predominantly oxygen-covered surface is very pronounced. Stopping the anodic scan at 965 mV, transient current oscillations evolved eventually falling off peak II as shown in Fig. 10(b). Note the extremely long poisoning process leading to a slow decrease of the current density followed by the very rapid increase in the current due to the removal of the poison. In Fig. 10(a), near the edge of peak II, where the $I-U$ curve abruptly falls off, some high-frequency small-amplitude spikes are also discernible in the observed CV. Similar spiking is observed during the time series of Fig. 10(b). For longer observation

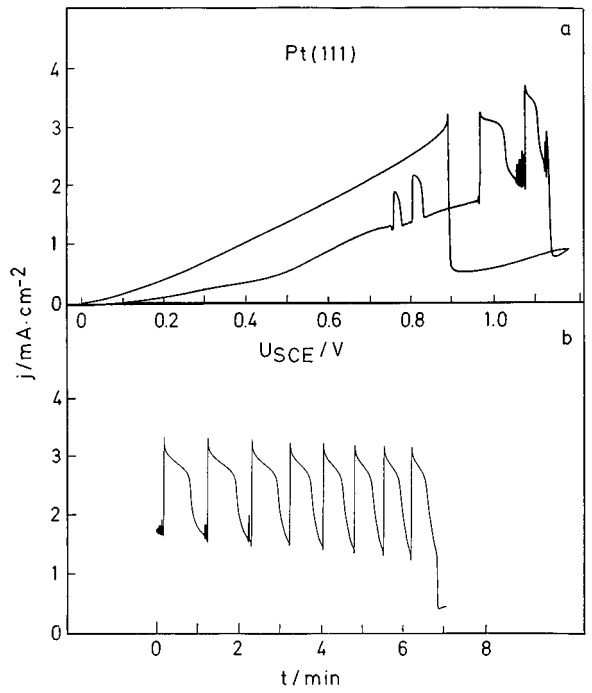

FIG. 10. (a) CV of FA oxidation on Pt(111) with external resistance $R_{ex}=430\ \Omega$ at low FA concentration. Bulk solution: 0.05 M HCOOH, 10^{-3} M $HClO_4$. Scan rate 5 mV/s. Broad current oscillations appear on the anodic scan only. (b) Current oscillations when the scan was stopped at 965 mV.

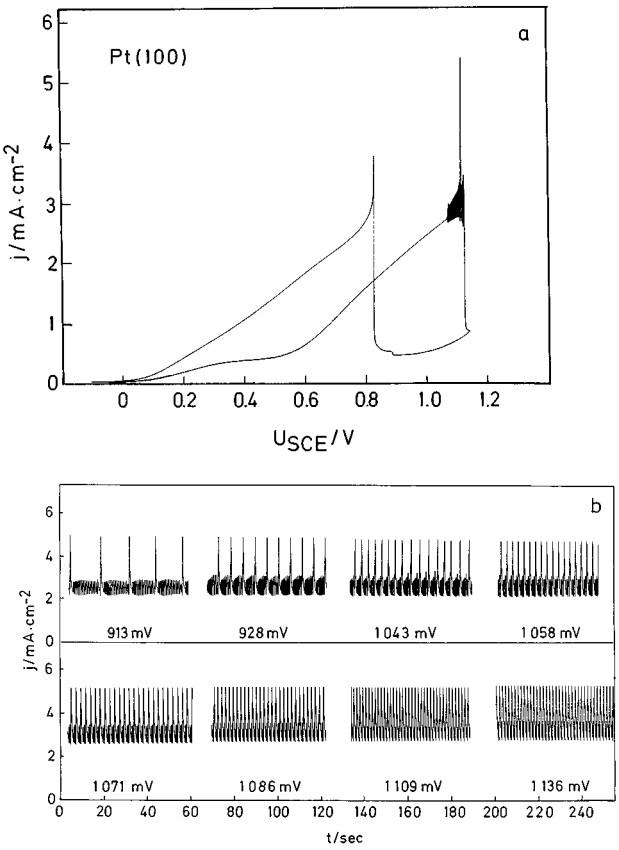

FIG. 11. (a) CV of FA oxidation on Pt(100) with external resistance $R_{ex}=390\ \Omega$ at high FA concentration. Bulk solution: 1 M HCOONa, 0.5 M H_2SO_4. Scan rate 5 mV/s. Small and large current spikes appear on the anodic scan only. (b) Mixed-mode oscillations at different constant potentials U.

times, however, this phenomenon seems to disappear as seen for the second portion of the time series in Fig. 10(b). It should be added that, especially for low HCOOH concentrations, oscillations on Pt(111) are comparatively difficult to obtain as has been stated by various authors.[16,17]

2. High HCOOH concentration

In addition to the current oscillations found on the low-index single crystal surfaces at low concentration, dynamical instabilities were also observed for considerably higher bulk concentration of HCOOH. The following experiments were performed in a supporting electrolyte containing 1 M HCOONa and 0.5 M H_2SO_4.

Pt(100). For $R_{ex}=390\ \Omega$ the (100) surface exhibits a rich variety of oscillatory states. Figure 11(a) displays the measured CV at 5 mV/s. Unlike the CV at low concentration, there is a broad potential region of visible large-amplitude current spikes on the cathodic flank of peak II. Looking at this region more closely further reveals that small high-frequency spikes appear between the large spikes which suggests the presence of mixed-mode oscillations. Stationary measurements of the current at different fixed potentials U confirmed the conjecture: Fig. 11(b) shows — for the first time to our knowledge — potentiostatic mixed-mode oscillations (MMOs) during the oxidation of formic acid.

For U below 1 V, the MMOs consist of a large current spike followed by a number of small-amplitude peaks (there are at least 14 small peaks at $U=0.913$ V). As U is further increased, the number of small spikes decreases until at $U=1.2$ V the system exhibits period-1 oscillations. At no parameter value of U did the dynamics resemble that close to a homoclinic orbit. In addition, no quasiperiodic regimes between two mixed-mode states could be identified. Instead, aperiodic mixed-mode regimes were found to exist in very narrow potential regions between two successive mixed-mode states.

Pt(110). At high concentration of HCOOH, both the $I-U$ characteristics and the shape of the transient current oscillations on the (110) surface were found to be very similar to what is shown in Fig. 9. Therefore, these results are not reported in detail.

Pt(111). Figure 12(a) displays the high-concentration CV obtained with 220 Ω on the (111) surface. The anodic potential sweep reveals regular large-amplitude current spikes on peak II. As with the low HCOOH concentration, no current spikes were observed in the reversed potential scan (except for very small scan rates). For $U=0.870$ V, regular current oscillations were observed [Fig. 12(b)] which considerably decreased in period length during the stationary measurement. As for their wave form, the oscillations are relaxation-type oscillations; as seen on Pt(100), this type of oscillation is characterized by the presence of different time scales on which the underlying chemical processes evolve.

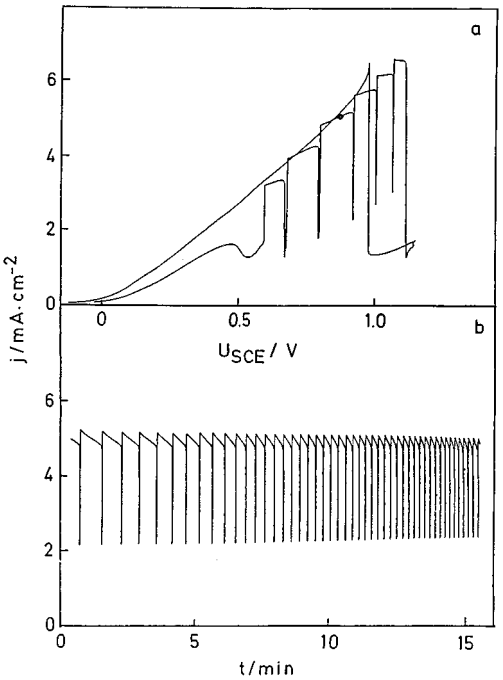

FIG. 12. (a) CV of FA oxidation on Pt(111) with external resistance $R_{ex}=220\ \Omega$ at high FA concentration. Bulk solution: 1 M HCOONa, 0.5 M H_2SO_4 . Scan rate 5 mV/s. Broad current oscillations appear on the anodic scan only. (b) Current oscillations when the scan was stopped at 870 mV.

The extremely rapid increase in current density is followed by an initially slow poisoning process which accelerates considerably for decreasing current densities. As found in Fig. 10(b), the oscillation period on Pt(111) was found to be much larger than for the other two surfaces. When the scan was stopped immediately past the reactivation of the surface while scanning cathodically, stable oscillations were found after a comparatively long transient. This shows that — similar to Pt(100) — oscillatory behavior is present in both scans, but is suppressed due to kinetic reasons.

D. Bifurcation behavior

In dynamical systems theory, parameter regions of distinct dynamics are conveniently shown in bifurcation diagrams. Varying a system parameter (called constraint for externally adjustable parameters) a bifurcation is said to occur if the behavior of a dynamical system changes qualitatively. Figure 13 shows such an experimental bifurcation diagram of the dynamics of the Pt(100) surface for a very low scan rate of the potential (5 mV/s). It should be noted that due to the finite potential sweep rate, Fig. 13 does not constitute a stationary bifurcation diagram as usually used in nonlinear dynamics. On the axes the two major constraints, the normalized external resistance $R_{ex}\cdot A$ (just denoted as RA in the figure) and the applied outer potential U, are plotted. The normalized resistance RA was chosen to be independent of individual electrode geometries. In Fig. 13, for a given value of RA, the minimal and maximal potential U at which current spikes were observed in the CV are indicated as solid lines regardless whether they were observed during the anodic or cathodic scan. Thus, for fixed parameter values of U and RA between the two solid lines, current oscillations can be observed. The dotted line indicates the rapid increase in current in the cathodic scan, corresponding to the regeneration of vacant surface sites by desorption of OH. Since the bifurcation diagram was recorded at low HCOOH concentrations, even without external resistance current oscillations occur.

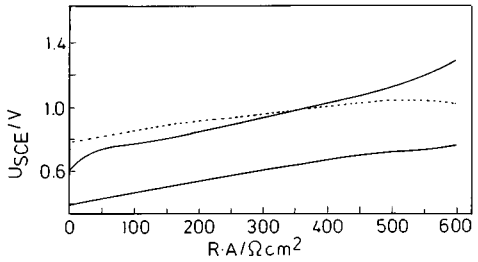

FIG. 13. Experimentally measured bifurcation diagram for Pt(100) in 0.05 M HCOOH, 10^{-3} M $HClO_4$. The lower and upper solid line denote the low-potential and high-potential transition points between stable current behavior and sustained current oscillations, respectively, as found when scanning with 5 mV/s. The dashed line displays the locations where the abrupt transition from low to high values of the current occurs when scanning cathodically.

E. Stirring effects on oscillations

In the following, the influence of stirring on current oscillations will be investigated. Figure 14(a) displays the observed effect of stirring on period 1 oscillation on the (100) surface at low HCOOH concentration. When stirring is turned on, the current oscillations remain stable, but change their shape. When stirring is stopped again, the current oscillations relax back to a shape similar to the initial one. In

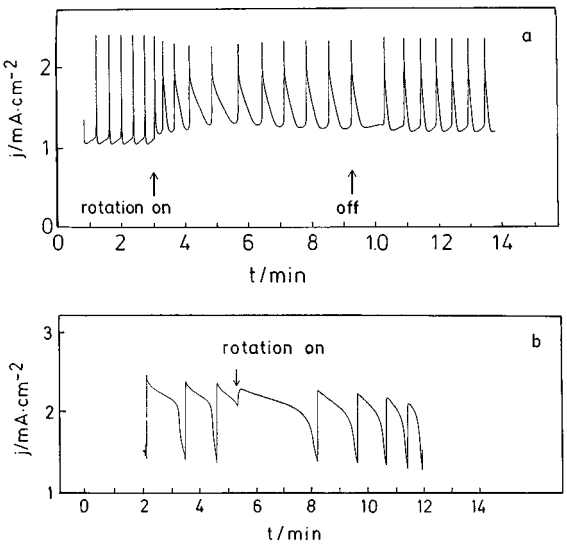

FIG. 14. Stirring effects on sustained period-1 oscillations (a) on Pt(100) in 0.05 M HCOOH, 10^{-3} M $HClO_4$, with $R_{ex}=600\ \Omega$ at $U=817$ mV, (b) on Pt(111) in 0.05 M HCOOH, 10^{-3} M $HClO_4$, with $R_{ex}=700\ \Omega$ at $U=1070$ mV. The period-1 oscillations survive when the stirring is switched on.

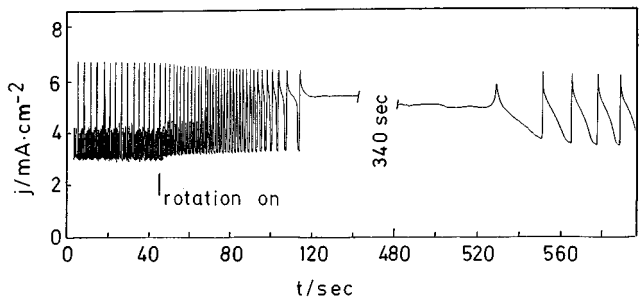

FIG. 15. Stirring effect on mixed-mode oscillations on Pt(100) in 1 M HCOONa, 0.5 M H_2SO_4 with $R_{ex}=280\ \Omega$ at $U=984$ mV. The mixed-mode oscillations are seen to be first quenched by stirring; after a transient, period-1 oscillations evolve.

Fig. 14(b), current oscillations on the (111) surface were subjected to stirring. As can be seen, stirring results in an initial phase delay of the oscillation period. Similar to Pt(100), the oscillations remain stable without considerable change of their wave form.

In Fig. 15 the effect of stirring on stable mixed-mode oscillations was investigated on the Pt(100) surface. Mixed-mode oscillations [see Fig. 11(b)] are subjected to stirring after 42 s (vertical line in Fig. 15). First, the mixed-mode character of the current oscillations vanishes by the disappearance of the small-amplitude peaks. Thereafter, the period 1 oscillations change their shape; the poisoning process becomes considerably delayed. About 80 s after starting the stirring, the distorted period 1 oscillations are suppressed completely for about 400 s. Finally, period 1 oscillations return which resemble those observed at low HCOOH concentration under stirring. The final period 1 oscillations are of a larger period compared to the initial mixed-mode oscillations. In order to rule out a simple parameter shift of the region of mixed-mode oscillations we investigated the system dynamics under stirred conditions for a variety of potentials U and of HCOOH concentrations. Mixed-mode oscillations, however, were never found with stirred electrolyte.

V. DISCUSSION AND MECHANISTIC CONSIDERATIONS

A. Role of the ohmic resistance *R*

In the previous section, we have reported a systematic investigation of dynamical instabilities occurring during formic acid oxidation on the three single crystal surfaces Pt(100), Pt(110) and Pt(111). We first emphasized the strong relation between electrochemical instabilities and the overall ohmic resistance R given by the sum of the ohmic resistance of the bulk solution and an externally applied resistance R_{ex}. Unfortunately, the important role of the ohmic resistance R and, accordingly, the role of the ionic concentration of the bulk solution were sometimes neglected in previous potentiostatic studies.[15–17,28] Figures 7(a) and 7(b) clearly show that it is the ohmic resistance R which accounts for the occurrence of electrochemical instabilities manifesting themselves in the case of formic acid not only by bistability, but due to appropriate slow chemical processes as sharp periodic current spikes [Figs. 6,7(a), and 7(b)]. The study further revealed that by application of an external ohmic resistance, new additional dynamic regimes are observable in the system. Moreover, we found that an external series resistor contributed considerably to the stability and reproducibility of the observed dynamics. This is seen by the well reproducible current oscillations on Pt(110) and Pt(111) as well as the potentiostatic mixed-mode regimes on Pt(100).

B. The CO-oxidation system

The electrochemical oxidation of CO can be considered as a simplified subsystem of the formic acid oxidation system involving similar surface oxidation reactions of the surface poison, but differing in the source of the poison. Therefore, the investigation of the CO oxidation can provide valuable information on the reactivity of CO with oxygen containing species on the three Pt single crystals.

Although the scanned CVs (Fig. 1) suggest the presence of a bistability in the system, the quasistationary (Fig. 1) and galvanostatic measurements indicate that the hysteresis is merely due to a slow CO adsorption process. If at all, true bistability only occurs in the absence of stirring.

An important conclusion from the foregoing discussion is that the CO oxidation system appears to be monostable for each single crystal. Consequently, a truly potentiostatic, i.e., purely chemical, instability — although feasible — seems not to be present. This result rules out certain suggestions as to the source of the instability of the formic acid system which has been put forward by different authors.[9,29–32]

From the relative position of the CO removal peaks of the three surfaces, we further conclude that the CO poisoning of the surface becomes less pronounced in the order Pt(100), Pt(110) to Pt(111). A very dense monolayer of CO on Pt(100) obviously offers few bare sites for oxygen species to adsorb in contrast to Pt(111) where oxidation starts at smaller U.

The finite oxidation current at high values of U indicates that the surface predominantly covered with OH allows for CO to be adsorbed and oxidized (asymmetric inhibition[33]).

C. A simple mechanism for the formic acid system

Most studies agree on the fact that formic acid oxidation proceeds via a dual path mechanism first proposed by Capon and Parsons.[20] According to these authors, the initial adsorption of formic acid is followed by the formation of a reactive intermediate (presumably $\cdot$COOH) which is immediately oxidated further to CO_2, the final product. The reaction steps can be formulated as

$$\mathrm{HCOOH}_{(aq)} \rightleftharpoons \mathrm{HCOOH}_{ad}, \tag{1}$$

$$\mathrm{HCOOH}_{ad} \rightarrow \mathrm{COOH}_{ad} + \mathrm{H}^+ + e^-, \tag{2}$$

$$\mathrm{COOH}_{ad} \rightarrow \mathrm{CO}_2 + \mathrm{H}^+ + e^-, \tag{3}$$

thereby assuming the oxidation of hydrogen radicals to be very fast. The rate of reaction (2) is certainly lower than that of reaction (3) since radical species are involved, but may be of comparable size to the adsorption reaction (1) depending

on the diffusion thickness, the concentration of HCOOH and the number of available free surface sites. The reaction path given by reactions (2) and (3) is usually referred to as the direct path of formic acid oxidation. It is important to note that it is this reaction path which provides the necessary current density to account for the measured current peaks.

The dual path mechanism[20] furthermore postulates a parallel reaction path to CO_2 via an intermediate which blocks the surface and impedes further adsorption of HCOOH. The nature of this poisoning species has long been the subject of intensive speculations.[24,34–37] Recent *in situ IR* spectrometry, however, gave cause for the belief that the dominating poisoning species is CO.[23–25] In the present study, we follow the most recent results and assume CO_{ad} to be the only poison involved.[17] The poisoning reaction is assumed to follow the simple scheme

$$HCOOH_{ad} \rightarrow CO_{ad} + H_2O. \tag{4}$$

At higher potential, CO_{ad} is assumed to be removed through a surface reaction with adsorbed OH stemming from the oxidation of water molecules:

$$H_2O \rightleftharpoons OH_{ad} + H^+ + e^-, \tag{5}$$

$$OH_{ad} + CO_{ad} \rightarrow CO_2 + H^+ + e^-. \tag{6}$$

Reactions (4)–(6) are usually referred to as the indirect path of formic acid oxidation. Several authors[9,29–32] assumed the kinetics of reaction (6) to involve an additional free surface site in order to account for an autocatalytic feedback, which in turn may cause a kinetic instability. In view of our results of the previous paragraph, however, we consider any additional kinetic assumption as irrelevant to the origin of oscillatory instabilities in the formic acid system. Again, we follow a simple mechanism and at this point neglect any further oxygen species such as PtO,PtO_2 or PtO(O)[20,38,39] and subsurface hydroxide and oxygen[40] which were postulated to occur at double layer potentials $\phi_{dl} > 1.0$ V. This simplification for the interpretation of oscillations can be justified as follows: Correcting the observed current oscillations by the *IR* drop as given in Section III one obtains the ''real'' potential oscillations across the double layer ϕ_{dl}. One finds that all current oscillations at fixed U observed in this study correspond to oscillations of ϕ_{dl} in the range of 0.1–0.7 V.

As mentioned in Section I, a region of negative differential resistance (NDR) is generally required for instability. Using the chemical reactions given above the occurrence of the NDR can now be made plausible. Whereas the direct oxidation path [reactions (1), (2), and (3)] shows a global positive potential characteristic, i.e., an increasing reaction rate as the applied potential is increased (positive slope of the I/U curve), the combination of the direct path and reaction (5) leads to an N-shaped $I-U$ curve showing a region of NDR (negative slope). This is due to the OH poisoning of the surface which decreases the number of free sites available for the direct oxidation path.

With the chemical (pseudo)reactions given above a plausible simple model is obtained which should, in principle, be able to qualitatively account for the occurrence of oscillatory instabilities. We now turn to a more detailed discussion of the current peaks observed in the CV and try to come up with a plausible interpretation in terms of the chemical reaction steps of the simple model.

D. Peak I and II

For $-0.1\ \text{V} < U < 0.5\ \text{V}$, i.e., the potential range of peak I, the residual number of free surface sites determines the rate of the direct oxidation path and simultaneously the measured current density on all three surfaces. For values of $U > 0.5$ V, OH is adsorbed on the surface [reaction (5)] regenerating an increasing number of free surface sites via reaction (6). Thus, the rate of the direct path increases considerably. As U increases further, all poisoning CO is removed, and the surface becomes blocked by the OH species. This scenario is believed to equally hold for all three surfaces during the anodic scan. Figure 3, however, shows pronounced discrepancies between the surfaces during cathodic sweeping which can be made plausible as follows: Pt(111) exhibits a lower affinity towards CO thus showing incomplete poisoning by CO[19,41,42] (see also the results on CO oxidation). In contrast, Pt(100) was found to be completely blocked by the poisoning species.[19,41,42] Furthermore, the direct path was also found to proceed faster on Pt(100) than on Pt(111).[42] This structural difference leads to a vanishing peak I, but to a pronounced peak II for Pt(100). The reverse, however, holds true for Pt(111). Pt(110) appears to behave similarly towards Pt(100). It should be noted that the CV of Pt(111) in Fig. 3(a) differs from those measured in previous studies[18,19] in that the current density of peak IV/V in the cathodic scan was found to be much larger than that of peak I in the anodic scan.

E. Peaks IV and V

In Section IV, we have shown the splitting of the large current peak on the cathodic scan of Pt(100) and Pt(110) into peaks IV and V and mentioned results on the dependence of these peaks on the scan rate and anodic reverse potential. By means of our simple model mechanism, we interpret the rapid current increase during the cathodic scan as the very rapid regeneration of a large number of free surface sites resulting in a high rate of the direct oxidation path. As U decreases, the surface becomes more and more poisoned by CO via reaction (4) until the current density vanishes. This qualitative interpretation is equally valid for all three surfaces and therefore does not account for the structural effects leading to the two distinct peaks IV and V. It is obviously necessary to reconsider possible additional reaction steps which are consistent with our experimental findings.

The dependence of peak IV on the upper limit potential shows a relationship between the amount of deposited oxygen species and peak IV. Compared to adsorption, the desorption of the oxygen species requires a smaller potential. Consequently, there is an overlap of the potential regions where the surface oxygen species are still present, yet where formic acid restarts to deposit on bare sites. From this, it is plausible to identify peak IV with the reaction of re-adsorbed

HCOOH and reactive surface oxides which remained on the surface. We therefore consider an additional chemical reaction step such as

$$HCOOH_{ad} + Pt-OH \rightarrow H_2O + CO_2 + Pt + H^+ + e^- \qquad (7)$$

to be involved in the chemical processes occurring at peak IV. The experimental finding that peak IV increases with increasing scan rate is consistent with the assumption that at least a part of the charge transfer involves preadsorbed species. Peak V almost coincides with peak I in potential suggesting its origin to be the direct oxidation path as discussed for peak I [reactions (2) and (3)].

It follows that peak IV originates in the oxidation of FA in the presence of adsorbed oxygen species, whereas peak V stems from the direct FA oxidation while at the same time the surface becomes slowly poisoned by CO.

1. Oscillatory instabilities

We have shown oscillatory behavior of the current density on the three low-index Pt single crystals at both low and high HCOOH concentrations. In general, current oscillations at high HCOOH concentration proved to be more stable and better reproducible than at low concentrations.

On the basis of the experimental results, the occurrence of the current oscillations can be described in physicochemical terms as follows: For an appropriate constant outer potential U and a sufficiently large ohmic resistance R, the total current density I based on the direct oxidation path decreases due to CO poisoning of the active surface. Therefore, the initially low double layer potential $\phi_{dl} = U - IR$ increases leading to the adsorption of OH. Due to OH_{ad} even more sites are blocked, which in turn lowers the current, increases ϕ_{dl}, enhances OH formation and leads to an overshooting of ϕ_{dl} on a fast time scale. Then, the reactive removal of CO (indirect path) sets in, regenerating vacant surface sites. This results in an increase of I and, due to the electrical relation given above, in a decrease of ϕ_{dl} until all OH has desorbed and the slow CO poisoning process resumes.

In Section IV, it was shown that the oscillatory potential range as well as the wave form of the current oscillations were very similar on both the cathodic and the anodic scan. This suggests that the oscillations on either scan are caused by the same instability. However, why is it that oscillatory spikes are visible over a broad potential range on the cathodic scan, but hardly appear on the anodic scan? The reason must be sought in the different initial conditions that hold when the double layer potential enters the unstable potential range. On the anodic scan, the surface is almost completely blocked by CO. Therefore, the CO coverage is too high for sustained oscillations to occur. Scanning anodically, a slow removal of CO by adsorbed OH occurs on the cathodic flank of peak II. Still, the transient behavior of the current, i.e., the time until the coverages of CO and OH necessary for oscillations are reached, is long compared to the time the system needs to leave the oscillatory potential range at the chosen sweep rate. Thus, no current spikes are seen scanning in the anodic direction. On the reversed scan, however, a large number of free surface sites is rapidly regenerated after the first OH desorption peak. Since on Pt(100) the rate of poisoning is high,[19,41,42] the time to reach the CO coverage necessary for oscillations is short compared to the time the system spends in the oscillatory potential region. Consequently, sharp current spikes are visible.

On Pt(111), the rate of poisoning (process 4) is comparatively slow[19,41,42] leading to the characteristic oscillatory wave form shown in Figs. 10(b) and 12(b). The low affinity of Pt(111) towards CO can also be used to explain the absence of current spikes on the cathodic scan [see Figs. 10(a) and 12(a)]. The reasoning is similar to that discussed for Pt(100): As soon as the surface becomes reactivated [at $U = 0.9$ V in Fig. 10(a), at $U = 0.95$ V in Fig. 12(a)], the double layer potential is too low for oscillations to occur due to the high IR drop. Now, the transient time until the CO coverage has reached the threshold value necessary for current oscillations is long compared to the time the systems spends in the oscillatory potential region. Further evidence in favor of this interpretation is provided by the experimental finding that current oscillations eventually evolve if the cathodic sweep is stopped after reactivation. Compared to Pt(100), current oscillations on Pt(111) are in general less stable and show transient behavior over a considerable potential range ending up on the OH-poisoned state. In general, the presence and absence of current spikes depends on the relative rate of scanning and induction of oscillations.

The findings on Pt(110) [Fig. 9(a)] best allow a conclusion on the type of bifurcations that leads to oscillatory instabilities. At the lower limit of the oscillatory potential region ($U = 0.68$ V), oscillations emerge with very small amplitude and high frequency suggesting a Hopf bifurcation as conjectured in the case of Pt(100). At the upper limit, however, the relaxation oscillations disappeared at finite amplitude and long period. From nonlinear dynamics it is well known that this is typical for a saddle-loop bifurcation. Similar to Pt(111) at low HCOOH concentration, the oscillations are transient and die on the low current branch.

At higher HCOOH concentrations, the (100) surface was found to exhibit a sequence of mixed-mode oscillations (MMOs) characterized by large current spikes followed by an increasing number of small high-frequency spikes for lower values of the applied potential U. This is — to our knowledge — the first observation of MMOs during formic acid oxidation under potentiostatic control. Previous work on formic acid dealing with MMOs focused mainly on galvanostatic conditions.[30–32]

From the experimental findings it would be daring to settle the question of what type of bifurcation scenario leads to the formation of mixed-mode oscillations. We can, however, certainly assume an additional negative feedback variable (chemical species) to be crucial to the dynamics which, together with the negative and the positive feedback involved in the period-1 oscillations, gives rise to two interacting oscillators and consequently to mixed-mode oscillations.

2. Stirring effects

Regardless of the orientation of the single crystal surfaces, period-1 oscillations during formic acid oxidation were found to survive while stirring. This is in agreement with early work on polycrystalline Pd,[9] but in contrast to recent results on Pt(100),[16] where stirring was found to suppress sustained oscillations. On Pt(100), the oscillatory wave form proved sensitive towards stirring in that it became less relaxational; the emerging oscillatory wave form resembled that which was found if, under unstirred conditions, one scanned to smaller potentials U. Thus, the set of chemical species essential to the oscillatory period-1 instability seems not to include any solution species as, at higher stirring rates, the solution species near the double layer become either quenched to their bulk concentration due to rapid mass transport or are rapidly removed from the surface.

From the global disappearance of mixed-mode oscillations on Pt(100) when subject to stirring, we can conclude that the set of chemical species essential for the occurrence of the small-amplitude spikes does involve at least one solution species. In view of the foregoing discussion on the origin of the MMOs we could identify this solution species as a candidate for an additional (negative-feedback) species essential for the dynamics of MMOs, but nonessential for period-1 oscillations. Under stirred conditions this solution species is not available as a dynamical variable so that only period-1 oscillations remain. The long transient before stable oscillations return is presumably the consequence of slowly reestablishing concentration conditions near the double layer necessary for oscillations.

[1] E. Müller and S. Tanaka, Z. Elektrochem. **34**, 256, (1928).
[2] W. Wolf, M. Lübke, M.T.M. Koper, K. Krischer, M. Eiswirth, and G. Ertl, J. Electroanal. Chem. **399**, 185 (1995).
[3] H. Degn, J. Chem. Soc. Faraday Trans. **64**, 1348 (1968).
[4] R. De Levie, Electroanal. Chem. Interfac. Electrochem. **25**, 257 (1970).
[5] M. T. M. Koper and J. H. Sluyters, Electroanal. Chem. and Interfac. Electrochem. **303**, 73 (1991).
[6] M. T. M. Koper, Electrochim. Acta **37**, 1771 (1992).
[7] M. T. M. Koper and J. H. Sluyters, J. Electroanal. Chem. **371**, 149 (1994).
[8] M. T. M. Koper and J. H. Sluyters, Electroanal. Chem. Interfac. Electrochem. **352**, 51 (1993).
[9] J. Wojtowicz, N. Marincic, and B. E. Conway, J. Chem. Phys. **48**, 4333 (1968).
[10] J. O'M Bockris, B. E. Conway, E. Yeager, and R. E. White, *Comprehensive Treatise of Electrochemistry* (Plenum, New York, 1981), Vol. 3.
[11] R. R. Adzic, in *Modern Aspects of Electrochemistry*, edited by R. E. White and J. O'M Bockris (Plenum, New York, 1990), Vol. 21.
[12] R. R. Adzic, A. V. Tripkovic, and W. O. Grady, Nature(London) **196**, 137 (1982).
[13] R. R. Adzic, W. O. Grady, and S. Srinivasan, Surf. Sci. **94**, 2191 (1980).
[14] J. Clavilier, J. Electroanal. Chem. **107**, 201 (1980).
[15] F. Raspel, R. J. Nichols, and D. M. Kolb, J. Electroanal. Chem. **286**, 279 (1990).
[16] F. Raspel and M. Eiswirth, J. Phys. Chem. **98**, 7613 (1994).
[17] N. Markovic and P. N. Ross, J. Phys. Chem. **97**, 9771 (1993).
[18] H. Kita and H. W. Lei, J. Electroanal. Chem. **388**, 167 (1995).
[19] A. Tripkovic, K. Popovic, and R. R. Adzic, J. Chim. Phys. **88**, 1635 (1991).
[20] A. Capon and R. Parsons, Electroanal. Chem. Interfac. Electrochem. **44**, 239 (1973).
[21] D. Dickertmann, F. D. Koppitz, and J. W. Schultze, J. Electroanal. Chem. **21**, 967 (1979).
[22] K. Yamamoto, D. M. Kolb, and R. Kötz, J. Electroanal. Chem. **96**, 233 (1979).
[23] R. Parsons and T. VanderNoot, J. Electroanal. Chem. **257**, 9 (1988).
[24] B. Beden, C. Lamy, N. R. D. Tacconi, and A. J. Arvia, Electrochim. Acta **35**, 691 (1990).
[25] B. Beden, J. M. Leger, and C. Lamy, in *Modern Aspects of Electrochemistry* (Plenum, New York, 1992), Vol. 22, p. 97.
[26] H. Okamoto, Electrochim. Acta **37**, 37 (1992).
[27] O. G. Tyurikova, N. B. Miller, A. A Yakovleva, and V. I. Veselovskii, Elektrokhim. **7**, 690 (1971).
[28] B. Beden, C. Lamy, and A. Bewick, J. Electroanal. Chem. **121**, 115 (1981).
[29] X. Cai and M. Schell, Electrochim. Acta **37**, 673 (1992).
[30] Y. Xu and M. Schell, J. Phys. Chem. **94**, 7137 (1990).
[31] M. Schell, F. N. Albahadily, J. Safar, and Y. Xu, J. Phys. Chem. **93**, 4806 (1989).
[32] F. N. Albahadily and M. Schell, J. Electroanal. Chem. **308**, 151 (1991).
[33] K. Krischer, M. Eiswirth, and G. Ertl, J. Chem. Phys. **96**, 9161 (1992).
[34] J. Willsau and J. Heitbaum, Electrochim. Acta. **31**, 843 (1986).
[35] O. Wolter, J. Willsau, and J. Heitbaum, J. Electrochem. Soc. **132**, 1635 (1985).
[36] B. Beden, A. Bewick, and C. Lamy, J. Electroanal. Chem. **150**, 505 (1983).
[37] B. Beden, A. Bewick, and C. Lamy, J. Electroanal. Chem. **148**, 147 (1983).
[38] S. Gilman, Electrochim. Acta **9**, 1025 (1964).
[39] B. E. Conway and S. Gottesfield, J. Chem. Soc. Faraday Trans. I **69**, 1090 (1973).
[40] H. Angerstein-Kozlowska, B. E. Conway, and W. B. A. Sharp, Electroanal. Chem. Interfac. Electrochem. **43**, 9 (1973).
[41] S. G. Sun, J. Clavilier, and A. Bewick, J. Electroanal. Chem. **240**, 147 (1988).
[42] S. Motoo and N. Furuya, J. Electroanal. Chem. **184**, 303 (1985).